Growth of Single-Walled Carbon Nanotubes from Sharp Metal Tips

*Julio A. Rodríguez-Manzo, Izabela Janowska, Cuong Pham-Huu, Antti Tolvanen, Arkady V. Krasheninnikov, Kai Nordlund, and Florian Banhart**

The nucleation and growth of single-walled carbon nanotubes is observed in situ in a transmission electron microscope. Carbon atoms are implanted into catalytically active metal particles by electron-beam sputtering. The metal particles are then shaped with a focused electron beam. Once the particles have a region of high surface curvature, spontaneous nucleation and growth of single-walled carbon nanotubes occurs on the metal particles. It is shown that the local solubility of carbon in the metal determines the nucleation of nanotubes. This is confirmed by atomistic computer simulations treating the solubility of carbon in a metal particle as a function of the size of the system.

Keywords:
- carbon solubility
- electron microscopy
- metal nanoparticles
- nanotube growth
- single-walled carbon nanotubes

1. Introduction

Despite their outstanding electronic properties,[1] carbon nanotubes (CNTs) are still far from implementation into commercially available electronic devices. This is in part due to the lack of a technique for a reliable and reproducible growth of CNTs with a specific atomic structure and, thus, unique electronic properties. The precondition for the development of such a procedure is a thorough understanding of the mechanisms of nucleation and growth of carbon nanotubes from catalytically active metal particles. Nanotubes are fabricated mainly by chemical vapor deposition (CVD) techniques[2] but some aspects of the mechanism by which CNTs grow have been clarified recently by in situ electron microscopy studies.[3–11] Of particular importance is the growth of single-walled carbon nanotubes (SWNTs) on or from solid nanometer-sized metal crystals.[6–8,10] Although indications for the diffusive transport of carbon atoms through the bulk of the catalyst particles have been found,[7,10] the model of surface diffusion is more convincing from an energetic point of view and has been favored in recent studies.[3,12–15] The conditions for the nucleation of SWNTs are thus still not known in detail but knowledge of the conditions is indispensable for the development of a technique to produce SWNTs with a predefined and uniform atomic structure. Here we describe in situ transmission electron microscopy (TEM) experiments where SWNTs grow from catalytically active transition metal nanoparticles whose surface curvature changes during the observations. It is shown that growth occurs by the segregation of carbon atoms at the surface of highly curved metal crystals.

[*] Dr. J. A. Rodríguez-Manzo, Prof. F. Banhart
Institut de Physique et Chimie des Matériaux, UMR 7504
Université de Strasbourg
23 rue du Loess, 67034 Strasbourg (France)
E-mail: florian.banhart@ipcms.u-strasbg.fr

Dr. I. Janowska, Dr. C. Pham-Huu
Laboratoire des Matériaux
Surfaces et procédés pour la Catalyse
UMR 7515 CNRS
European Laboratory for Catalysis and Surface Sciences
ELCASS, 25 rue Becquerel, 67087 Strasbourg (France)

A. Tolvanen, Dr. A. V. Krasheninnikov, Prof. K. Nordlund
Materials Physics Division
University of Helsinki
P.O. Box 43, 00014 Helsinki (Finland)

Dr. A. V. Krasheninnikov
Laboratory of Physics
Helsinki University of Technology
P.O. Box 1100, 02015 Helsinki (Finland)

Supporting Information is available on the WWW under http://www.small-journal.com or from the author.

DOI: 10.1002/smll.200900590

2. Results

As has been shown in a recent study,[16] intense irradiation of metal-filled multi-walled carbon nanotubes (MWNTs) with a focused electron beam leads to the segregation of metal and

NANO MICRO small

graphitic material and to the formation of heterojunctions between MWNT segments and metal particles with covalent bonds at the metal–nanotube interfaces. This phenomenon was taken as the basis of the present study. MWNTs filled with crystalline rods of Co or Ni were synthesized by CVD.[17,18] An area of a MWNT that contained an encapsulated metal nanoparticle was irradiated with an intense electron beam (10^3–10^4 A cm^{-2}) at 600 °C in the heating stage of an electron microscope[19] to produce a MWNT–metal–MWNT heterojunction, where two MWNT segments are joined by the previously encapsulated particle, as shown in Figure 1A. These heterojunctions remain stable if irradiation is interrupted.

The metal particle that forms the link between two MWNTs was then shaped by sustained electron irradiation (>10^3 A cm^{-2}) with a focused beam on the centre of the metal particle. A slow but ongoing thinning of the metal occurred, leading to an hour-glass shape. The beam current density was then lowered to normal imaging conditions (<100 A cm^{-2}) before the metal particle broke at the bottleneck, as shown in Figure 1B. Immediately after the metal separated into two halves, a SWNT appeared, bridging the gap between the two metal cones and growing in length as the two tips separated from each other. After having reached a certain length, the SWNT stops growing and breaks (bottom of Figure 1B). The complete process is also shown in Movie 1 of the Supporting Information. The nanotube is in an end contact with the lattice of the metal, as shown in Figure 1C. It has to be emphasized that the metal crystal is not surrounded by a graphenic shell. Fringes around the metal appear in some images but are due to Fresnel diffraction and can easily be distinguished from graphenic layers by changing the focus of the objective lens (Fresnel fringes move whereas the image of the layers remains stationary). Figure 1 shows the growth of a SWNT from a Co crystal but the same effect was also observed for Ni and FeCo alloy crystals under similar conditions. During the process, the metal remained crystalline in the face-centered cubic (fcc) structure. The process was observed at various temperatures in the range 450–700 °C.

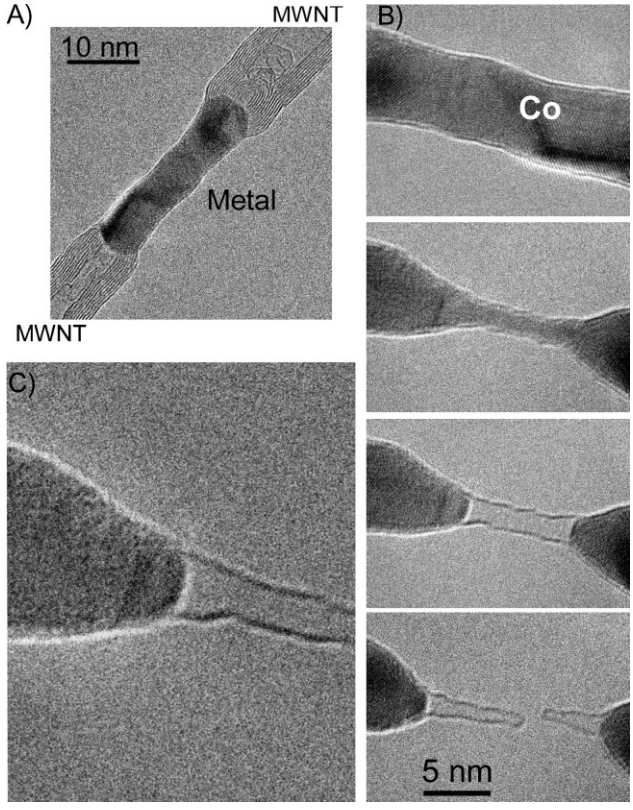

Figure 1. A) MWNT–Co–MWNT heterojunction formed by electron irradiation (200 keV) with high electron-beam current density (>10^3 A cm^{-2}) of a Co-filled MWNT at 600 °C; the Co particle connects two MWNT segments. B) Thinning of the center of the Co particle (joining two MWNT segments, not shown) under irradiation with an intense focused electron beam and breakage under irradiation with a low beam intensity at 600 °C. When the two metal tips separate from each other, a SWNT appears, bridging the metal segments. After a period of growth, the SWNT breaks. From top to bottom the elapsed times are 0, 767, 771, and 940 s, respectively. C) Interface between a SWNT and a metal crystal at higher magnification, taken 820 s after the first image in (B). The whole process is shown in detail in Movie 1 of the Supporting Information.

The growth of a SWNT was also witnessed when the disruption occurred at one of the MWNT–metal interfaces, as shown in Figure 2 for a MWNT–Co interface. The lattice image in Figure 2A shows the bonding between the metal particle and the MWNT. The metal is not covered with a visible graphenic shell. Under irradiation both the metal crystal and the MWNT shrank at the interface between the tube on the left-hand side and the metal. As the two components separated, a SWNT appeared, connecting the outermost layer of the MWNT with the metal tip.

The growth of a SWNT was not observed before the radius of curvature of the metal tip was smaller than 2–3 nm. Growth from a blunt surface with low curvature (large radius of curvature) did not occur. Figure 3A–D shows an example where the SWNT started growing from an isolated metal tip (after

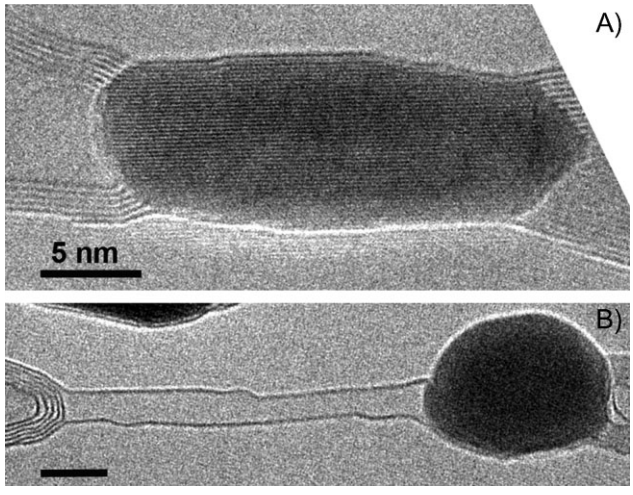

Figure 2. Growth of a SWNT at a MWNT–Co interface. The sample was irradiated with 200 keV electrons at 700 °C. A) MWNT–Co–MWNT heterojunction. The Co particle is in the crystalline state and the graphitic layers of the tube are directly connected to the metal lattice without a graphitic surface layer on the metal. B) After irradiating the interface between the MWNT on the left-hand side and the Co particle for 18 min with an intense beam, the metal particle detached and retracted from the MWNT and transformed to a spherical shape. During this process, a SWNT grew and bridged the gap between the Co particle and the MWNT. Scale bar: 5 nm.

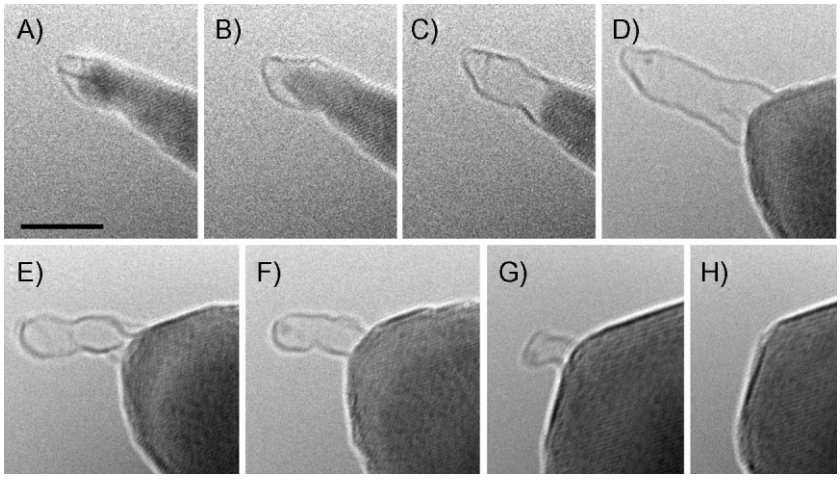

Figure 3. A–D) A SWNT grows from a sharp Ni tip that was obtained from a broken double-cone structure as in Figure 1B. SWNT growth is observed as long as the metal tip remains sharp. E–H) After rounding of the metal tip, it is observed that carbon material is re-ingested into the now blunt Ni particle. The image series was taken from a MWNT–Ni structure irradiated at 470 °C. During the process shown here the beam current density was less than 100 A cm^{-2}. From (A) to (H) the elapsed times are 0, 2, 4, 61, 127, 206, 360, and 387 s, respectively. Scale bar: 5 nm.

breakage of a double-cone structure, as shown in Figure 1). The sharp metal tips from where the SWNTs grew were found to be unstable. A transformation of the metal particle from a sharp cone to a nearly spherical shape (Figure 3) was observed and is due to a tendency towards reducing surface tension of the metal. The transformation of the metal had a considerable influence on the growth of SWNTs. It was observed that the SWNT remaining on the metal tip vanished rapidly once the radius of curvature of the metal particle increased. An example is shown in Figure 3E–H. The SWNT in this example grows from the metal tip as long as the tip remains sharp but stops growing or vanishes into the metal once the radius of curvature of the surface increases beyond a certain value (Movie 2 of the Supporting Information shows a recording of this process). Hence, it is obvious that SWNTs are only expelled from sharp metal tips (high surface curvature). The tubes disappear due to partial re-ingestion into blunt metal particles (low surface curvature) but possibly also due to electron-beam sputtering of carbon atoms.

The growth rate of the SWNTs was not constant in these experiments. The maximum was observed at the initial moments of nanotube formation, with values in the range of 0.2–2 nm s^{-1}. A plot showing the number of carbon atoms in a growing SWNT as a function of time is shown in Figure 4 for four different growth experiments where Co particles of different size were used. The nucleation and initial growth of the SWNTs was often too fast to be observed in detail within the time resolution of in situ TEM imaging (growth is much faster than indicated by the left slope of a curve connecting the first data points with the point at $t = 0$). Only in a few cases (as shown in Figure 3) could the growth be monitored in detail. The growth is followed by a period of an almost constant number of atoms in the nanotube. Afterwards, a decrease of the number of carbon atoms, mainly caused by diameter reduction, is observed before breakage of the nanotube occurs (encircled points in Figure 4). Stable SWNTs have been obtained, both before and after SWNT breakage. The initial size of the metal particle (before thinning) does not significantly influence the amount of carbon that is expelled from the SWNT, provided the experiment is carried out under similar conditions of irradiation and temperature, as Figure 4 shows. For example, two metal particles with an eightfold difference in volume (0.7×10^3 and 6.1×10^3 nm^3) produced two SWNTs with just a difference of less than a factor of 1.5 in carbon content (1.5×10^3 and 2.3×10^3 C atoms, respectively).

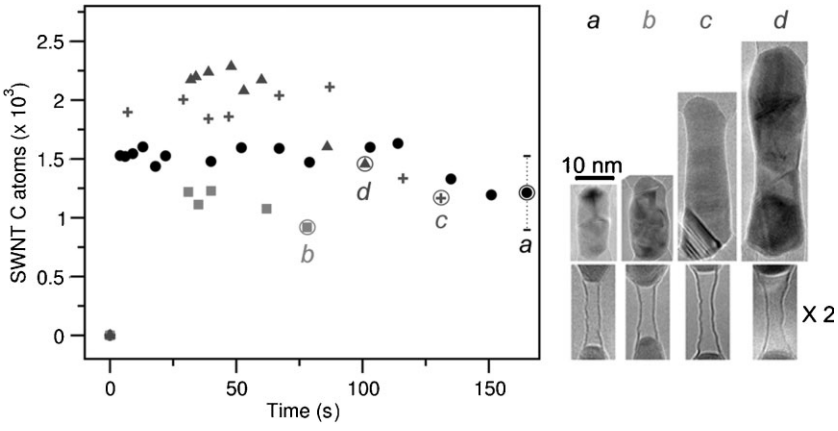

Figure 4. Estimated number of carbon atoms in SWNTs grown from four different Co particles as a function of time (assuming a SWNT surface density of 38.3 carbon atoms nm^{-2}). The points enclosed in circles mark SWNT rupture. The labels a–d indicate from which particle the data points were taken. The volumes of the starting metal particles were 0.7 (a), 1.3 (b), 3.1 (c) and 6.1 (d) $\times 10^3$ nm^3, respectively. The TEM was operated at 200 kV and the sample temperature was kept at 600 °C. Images of the starting Co particles as well as the SWNTs grown from them are shown on the right-hand side. Since the growth was too rapid to be monitored in detail, the growth speed cannot be extracted from the slopes of the curves (the first data points of the curves had to be taken at different times due to technical reasons).

3. Discussion

3.1. Implantation of Carbon Atoms into the Metal

The present experiment is different from standard CNT growth by CVD in so far as the supply of carbon atoms does not come from the decomposition of hydrocarbons at the metal surface. In a typical CVD experiment, SWNTs nucleate on small metal particles in such a way that a fullerenic cap is extruded from the spherical metal surface (root growth)[20] or that the metal particle stays on top of the growing SWNT.[21] In both cases, the metal tips

NANO MICRO small

have a diameter comparable to the diameter of the growing SWNTs. In the present experiment, the nucleation and growth dynamics of CNTs seem to occur in a related way. During the formation of a junction between two MWNTs and a metal particle, graphitic material that initially covered the metal crystals is implanted into the metal by knocks from the energetic electrons.[7,16] Furthermore, the metal crystal is connected to a MWNT from where mobile carbon atoms can be supplied. Since the MWNTs have been exposed to sustained irradiation before the metal–MWNT junction was formed, we can expect a certain number of mobile carbon interstitials in the MWNTs, in particular in their inner hollow.[22,23] These carbon atoms can be transferred through the metal particle by diffusion. Either of these processes leads to a gradual saturation of the metal crystals with carbon atoms. Since there is a transfer of carbon into the metal but the solubility of carbon is low (in bulk Co < 0.5 atom. % for the temperature range 450–700 °C[24]), segregation of carbon at the surface must take place. The nucleation of SWNTs occurs once the metal crystal has transformed to such an extent that a region of high surface curvature appears. Considering the diffusivity of carbon in transition metals, average migration distances of approximately 150–250 nm per second for a carbon atom in bulk Co or Ni are expected at 600 °C.[25,26] Thus, bulk and surface diffusion is much faster than necessary for the migration of carbon through the metal particle within the time and length scales of the reported experiments.

3.2. Computational Treatment of Carbon Solubility in the Metal

In order to understand the nucleation and growth of SWNTs in the present experiment, we carried out atomistic computer simulations, aimed at assessing the solubility of carbon in nanoscale metal particles as a function of the size of the particles. We chose iron as a metal occurring in the fcc phase in nanometer-sized crystals, as produced during the synthesis of CNTs.[27] We have recently developed an analytical bond-order potential[28] that can describe various phases of Fe-C systems. The formation enthalpy H_f of a C interstitial in the metal (at zero temperature) is defined as[29]

$$H_f = E(\text{metal} + 1\text{C}) - E(\text{metal}) - E(\text{graphene}) \quad (1)$$

where $E(\text{metal} + 1\text{C})$ and $E(\text{metal})$ are the total energies of the metal system with and without a C interstitial, respectively, and $E(\text{graphene})$ is the energy per atom in graphene. As the energy of an isolated C atom is zero in our model, $E(\text{graphene})$ coincides with the cohesive energy of graphene, which is equal to 7.375 eV, in agreement with the experimental value of 7.36 eV.[30] We considered the octahedral interstitial, as its energy is lower than that of the tetrahedral interstitial. Our simulations for the bulk Fe-C system gave $H_f = 0.24$ eV. This value is not too far from the experimental value of 0.4 eV[31] (we note that density-functional theory simulations[32] gave a negative value of −0.1 eV). Besides, relative values related to the changes in the size of the system are important for our analysis.

We calculated H_f for C interstitials in cylindrical Fe rods of various diameters d, mimicking the experimental systems. Cylinders were carved from the bulk fcc lattice with three different orientations of the crystallographic axes with respect to the rod axis. We also calculated H_f for a spherical nanoparticle. The atomic co-ordinates of all atoms were fully relaxed with or without the presence of a C atom in an octahedral position in the unit cell closest to the centre of the system by the conjugate gradient method.

Figure 5 presents H_f as a function of system diameter for nanorods and nanoparticles. It is evident that the averaged value of H_f is higher in small systems and exceeds the value corresponding to the bulk limit of 0.24 eV. The dependence is non-monotonous. The fluctuations in energy are related to different surface areas of the systems that changed from configuration to configuration when more atoms were incorporated into the system. The higher values of H_f at lower diameter are consistent with recent reports on the reduced solubility of C in nanoscale metal systems.[33] This result can be associated with the stress field (extra pressure) created by the surface and acting on the interstitial. The stress fields calculated as in Reference [34] of the C interstitial (in the middle of the system) and extra pressure generated by the

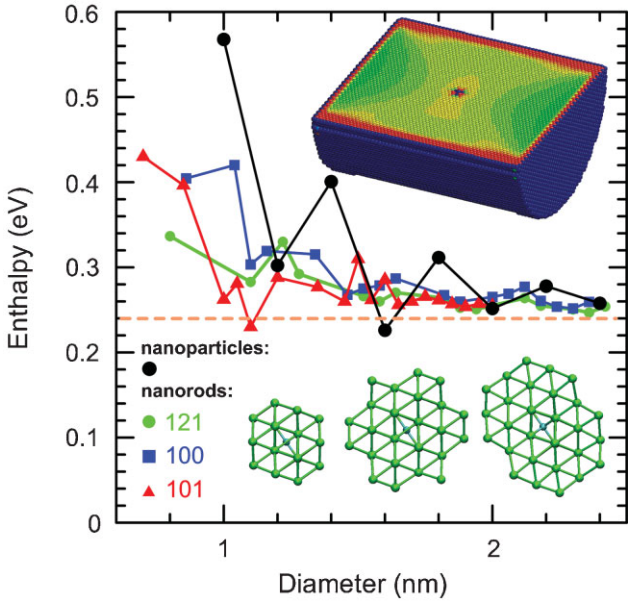

Figure 5. Calculated formation enthalpy H_f for a carbon interstitial on an octahedral site in fcc iron nanoparticles as a function of the particle diameter. Cylindrical rods (in green, blue, and red) and spherical particles (in black) are shown. The axis of the cylindrical rods coincides with the [121] (green curve), [100] (blue curve), and [101] (red curve) directions. The insets in the lower part of the image show examples of cross sections for [121] rods of different diameter. The changes in surface area cause the fluctuations in the enthalpy curves. It is evident that the averaged value of H_f for small rods exceeds the bulk limit value shown by the horizontal dashed line. Higher values of H_f originate from the additional pressure induced by the surface, as illustrated in the upper inset, which presents a part of the rod with the atoms colored according to the algebraic sum of virials calculated for each atom along three main axes. Red color corresponds to the highest pressure (exceeding 2 GPa), blue color to negative values (Fe–C bonds). Surface atoms are also shown in blue.

surface are shown in the upper part of Figure 5 for a cylinder with a large d (≈8 nm). Red color means higher pressure (the lattice is contracted), blue lower (even negative pressure, corresponding to stretching). Surface atoms should not be taken into account in the analysis. Negative pressure occurs at the C–Fe bonds only. The overlap of the stress fields generated by the interstitial and the surface for small d (<2 nm) results in an increase in H_f.

Assuming the averaged difference of $\Delta H \approx 0.1$ eV between the enthalpies for interstitials in rods with small ($d \approx 1.5$ nm) and large ($d > 3$ nm) diameters, as in the example shown in Figure 3A and D, the maximum concentration of carbon at the experimental temperature of $T = 470\,^{\circ}C$ (743 K) should be lower in the small rod by a factor of $\exp(\Delta H/kT) \approx 5$. Assuming that a metal crystal is initially saturated with carbon, carbon should indeed precipitate in the areas with high curvature as the local diameter of the rod is getting smaller.

When the system changes from a sharp to a blunt tip, as shown in Figure 3, H_f drops by 0.1 eV, so the solubility of carbon increases again by a factor $\exp(\Delta H/kT)$, thus lowering the Gibbs free energy $G = nH–TS$ by incorporating carbon atoms from the nanotube into the metal particle. However, our estimates for the typical sizes of the re-ingested nanotube (composed of ≈1000 C atoms) and metal particles showed that the shape-changing part of the metal particle is not always big enough to accommodate all C atoms. Thus, contributions from irradiation-induced sputtering of the nanotube[35] and migration of carbon atoms on the surface,[23] followed by an accumulation of carbon in a different part of the system, are processes that also may contribute to the disappearance of the nanotube in Figure 3.

3.3. Contribution of Surface Diffusion Effects

The contribution of carbon atoms diffusing over the surface of the metal particle to CNT growth should also be taken into account. Since surface diffusion has a lower energy barrier than bulk diffusion, surface diffusion should be favorable. However, if surface migration of carbon atoms was responsible for the growth of SWNTs in the present experiment, the influence of surface curvature of the metal on the growth of tubes would be difficult to explain, and surface migration can, thus, only have a minor influence. A coherent carbon layer on the metal surface before the nucleation of the tube can be excluded until the diameter of the metal rod became comparable to the diameter of the growing tube.

The thinning of the metal particle under irradiation is based on known phenomena.[36] Since the electron energies in these experiments (200 keV) are insufficient to transfer enough momentum to Co or Ni atoms to cause bulk displacement,[19,37] surface effects must be responsible. According to our molecular dynamics simulations, the minimum threshold energy for the sputtering of surface metal atoms is about a factor of four lower than the minimum threshold energy for bulk defect production. Thus, the electron energy of 200 keV is indeed sufficient to cause sputtering of metal atoms. It appears that surface atoms become mobile after momentum transfer from the electrons but are attached to the metal surfaces outside the irradiated area. The equilibrium morphology of a small metal crystal would be a spherical shape, possibly having facets at the surface. Therefore, thin crystalline wires or sharp tips are unstable.[38] This effect appeared in the present experiment: once the double-cone structure broke, the sharp metal tips rounded slowly during the observation. The separation of the two halves of the system shows that a certain force acts in the axial direction during the experiment. This is due to the collapse of the MWNTs on both sides under the beam, leading to a shortening of the tubes. The axial stress might contribute to the final thinning of the metal particle.

4. Conclusions

We have shown the growth of SWNTs from highly curved surfaces of transition metal particles that are saturated with carbon. Sharp metal tips with a radius of curvature of less than approximately 3 nm are a necessary condition for nanotube growth. The results are consistent with the model of carbon diffusion through the bulk of the metal, but surface or subsurface diffusion cannot be excluded. The absence of a cap when the SWNT nucleates indicates that the SWNT structure is not necessarily defined by the formation of a cap with a certain size, and that the diameter and structure of the nanotube are controlled by the shape and size of the catalyst particle. The observed processes provide insight into the general mechanism of SWNT nucleation and growth and should also be applicable in CVD. New avenues of SWNT production can be envisaged, for example, pre-shaping of metal catalyst surfaces so that a well-defined starting condition for the nucleation of SWNTs with uniform structure and diameter can be achieved. In addition, this procedure can also be employed to study the properties of metal–SWNT heterojunctions.

5. Experimental Section

MWNTs partially filled with crystalline nanoparticles of Co or Ni were synthesized by CVD.[17,18] To produce Co-filled MWNTs, a saturated solution of Co II acetyl acetonate in ethanol was sprayed with argon into a furnace at 850 °C. The tubes were collected on standard Cu grids for electron microscopy. In-situ electron irradiation experiments were carried out in a transmission electron microscope operating at 200 kV (Jeol 2100F), equipped with an aberration corrector for the illumination system. The experiment was carried out in vacuum (no gases were supplied to the specimen chamber of the microscope). To avoid radiation-induced defect agglomeration in the graphitic shells, the samples were held at temperatures in the range of 450–700 °C in a heated specimen holder during the experiments in the TEM.[19] Images were recorded on a CCD camera with exposure times of 0.1–0.2 s. Time-lapse movies as shown in the Supporting Information were composed from single CCD exposures. Small time intervals were not available but the dynamics of the process can be visualized nevertheless.

Acknowledgements

Support from the Deutsche Forschungsgemeinschaft (BA 1884/6-1) and the Région Alsace (480-09) is gratefully acknowledged. This work was also supported by The Academy of Finland Centres of Excellence CMS and COMP. We also thank the Finnish IT Center for Science for generous grants of computer time. J.A.R.M. acknowledges IPICYT laboratory for assistance in the Ni sample synthesis. A.V.K. acknowledges support from the European Commission under the 6 Framework Programme STREP (Project BNC Tubes, Contract No. NMp4-CT-2006-033350).

[1] R. Saito, G. Dresselhaus, M. S. Dresselhaus, *Physical Properties of Carbon Nanotubes*, Imperial College Press, London **1998**.
[2] E. Joselevich, H. Dai, J. Liu, K. Hata, *Carbon Nanotubes: Advanced Topics in the Synthesis, Structure, Properties, and Applications*, (Eds: A. Jorio, G. Dresselhaus, M. S. Dresselhaus), Springer, Berlin **2008**.
[3] S. Helveg, C. López-Cartes, J. Sehested, P. L. Hansen, B. S. Clausen, J. R. Rostrup-Nielsen, F. Abild-Pedersen, J. K. Nørskov, *Nature* **2004**, *427*, 426.
[4] R. Sharma, Z. Iqbal, *Appl. Phys. Lett.* **2004**, *84*, 990.
[5] K. Jensen, W. Mickelson, W. Han, A. Zettl, *Appl. Phys. Lett.* **2005**, *86*, 173107.
[6] M. Lin, J. P. Ying Tan, C. Boothroyd, K. P. Loh, E. S. Tok, Y. Foo, *Nano Lett.* **2006**, *6*, 449.
[7] J. A. Rodríguez-Manzo, M. Terrones, H. Terrones, H. W. Kroto, L. Sun, F. Banhart, *Nat. Nanotechnol.* **2007**, *2*, 307.
[8] S. Hofmann, R. Sharma, C. Ducati, G. Du, C. Mattevi, C. Cepek, M. Cantoro, S. Pisana, A. Parvez, F. Cervantes-Sodi, A. C. Ferrari, R. Dunin-Borkowski, S. Lizzit, L. Petaccia, A. Goldoni, J. Robertson, *Nano Lett.* **2007**, *7*, 602.
[9] M. Lin, J. P. Y. Tan, C. Boothroyd, K. P. Loh, E. S. Tok, Y. Foo, *Nano Lett.* **2007**, *7*, 2234.
[10] H. Yoshida, S. Takeda, T. Uchiyama, H. Kohno, Y. Homma, *Nano Lett.* **2008**, *8*, 2082.
[11] C. Jin, K. Suenaga, S. Iijima, *ACS Nano* **2008**, *2*, 1275.
[12] S. Hofmann, G. Csányi, A. C. Ferrari, M. C. Payne, J. Robertson, *Phys. Rev. Lett.* **2005**, *95*, 036101.
[13] F. Abild-Pedersen, J. Norskov, J. Rostrup-Nielsen, J. Sehested, S. Helveg, *Phys. Rev. B* **2006**, *73*, 115419.
[14] H. Amara, C. Bichara, F. Ducastelle, *Phys. Rev. Lett.* **2008**, *100*, 056105.
[15] O. V. Yazyev, A. Pasquarello, *Phys. Rev. Lett.* **2008**, *100*, 156102.
[16] J. A. Rodríguez-Manzo, F. Banhart, M. Terrones, H. Terrones, N. Grobert, P. M. Ajayan, B. G. Sumpter, V. Meunier, M. Wang, Y. Bando, D. Golberg, *Proc. Natl. Acad. Sci. U. S. A.* **2009**, *106*, 4591.
[17] A. L. Elías, J. A. Rodríguez-Manzo, M. R. McCartney, D. Golberg, A. Zamudio, S. E. Baltazar, F. López-Urías, E. Muñoz-Sandoval, L. Gu, C. C. Tang, D. J. Smith, Y. Bando, H. Terrones, M. Terrones, *Nano Lett.* **2005**, *5*, 467.
[18] I. Janowska, G. Wine, M. Ledoux, C. Pham-Huu, *J. Mol. Catal. A-Chem.* **2007**, *267*, 92.
[19] F. Banhart, *Rep. Prog. Phys.* **1999**, *62*, 1181.
[20] J.-Y. Rati, F. Gygi, G. Galli, *Phys. Rev. Lett.* **2005**, *95*, 096103.
[21] H. Dai, A. G. Rinzler, P. Nikolaev, A. Thess, D. T. Colbert, R. E. Smalley, *Chem. Phys. Lett.* **1996**, *260*, 471.
[22] F. Banhart, J. Li, A. V. Krasheninnikov, *Phys. Rev. B* **2005**, *71*, 241408.
[23] Y. Gan, J. Kotakoski, A. V. Krasheninnikov, K. Nordlund, F. Banhart, *New J. Phys.* **2008**, *10*, 023022.
[24] M. Hasebe, H. Ohtani, T. Nishizawa, Metall, *Mater. Trans. A* **1985**, *16*, 913.
[25] W. Moffatt, *The Handbook of Binary Phase Diagrams*, Genium Publishing Corporation, New York **1976**.
[26] J. Lander, H. Kern, A. Beach, *J. Appl. Phys.* **1952**, *23*, 1305.
[27] B. Wei, M. Shima, R. Pati, S. K. Nayak, D. J. Singh, R. Ma, Y. Li, Y. Bando, S. Nasu, P. M. Ajayan, *Small* **2006**, *2*, 804.
[28] K. O. E. Henriksson, K. Nordlund, *Phys. Rev. B* **2009**, *79*, 144107.
[29] C. Domain, C. S. Becquart, J. Foct, *Phys. Rev. B* **2004**, *69*, 144112.
[30] C. Kittel, *Introduction to Solid-State Physics*, Wiley, New York **1996**.
[31] J. A. Lobo, G. H. Geiger, *Metall. Mater. Trans. A* **1976**, *7*, 1347.
[32] D. E. Jiang, E. A. Carter, *Phys. Rev. B* **2003**, *67*, 214103.
[33] A. R. Harutyunyan, N. Awasthi, A. Jiang, W. Setyawan, E. Mora, T. Tokune, K. Bolton, S. Curtarolo, *Phys. Rev. Lett.* **2008**, *100*, 195502.
[34] J. Kotakoski, A. V. Krasheninnikov, K. Nordlund, *Phys. Rev. B* **2006**, *74*, 245420.
[35] A. V. Krasheninnikov, F. Banhart, J. X. Li, A. S. Foster, R. M. Nieminen, *Phys. Rev. B* **2005**, *72*, 125428.
[36] R. F. Egerton, F. Wang, P. A. Crozier, *Microsc. Microanal.* **2006**, *12*, 65.
[37] R. F. Egerton, P. Li, M. Malac, *Micron* **2004**, *35*, 399.
[38] V. Rodrigues, T. Fuhrer, D. Ugarte, *Phys. Rev. Lett.* **2000**, *85*, 4124.

Received: April 8, 2009
Revised: August 7, 2009
Published online: September 9, 2009

